Carbohydrate Polymers 118 (2015) 133–142

Contents lists available at ScienceDirect

Carbohydrate Polymers

journal homepage: www.elsevier.com/locate/carbpol

PCL/chitosan/Zn-doped nHA electrospun nanocomposite scaffold promotes adipose derived stem cells adhesion and proliferation

Fereshteh Mohammad Ghorbani [a], Babak Kaffashi [a], Parvin Shokrollahi [b,*], Ehsan Seyedjafari [c], Abdolreza Ardeshirylajimi [d]

[a] Department of Polymer Engineering, University of Tehran, Tehran, Iran
[b] Department of Biomaterials, Iran Polymer and Petrochemical Institute, Tehran, Iran
[c] Department of Biotechnology University of Tehran, Tehran, Iran
[d] Stem Cell Technology Research Center, Tehran, Iran

ARTICLE INFO

Article history:
Received 30 May 2014
Received in revised form
27 September 2014
Accepted 23 October 2014
Available online 20 November 2014

Keywords:
Polycaprolactone
Chitosan
Zn-doped nanohydroxyapatite
Tissue engineering
Electrospun scaffold

ABSTRACT

Chitosan (Ch), and poly(ε-caprolactone) (PCL), widely used as biomaterials with desirable properties for tissue engineering applications, were both blended with zinc-doped hydroxyapatite nanoparticles(nZnHA) and electrospun into nanofibrous scaffolds using formic acid/acetic acid. The rationale behind this study was to demonstrate that presence of small quantities of Zn^{2+} ions doped in HA nanoparticles can improve biocompatibility of PCL/Ch blends. SEM observation revealed that average fiber diameter was increased from about 136 nm for a PCL/Ch blend, to around 210 nm for PCL/Ch/nZnHA nanocomposite. PCL/Ch/nZnHA scaffolds offered higher elastic modulus (about 3-fold) and tensile strength (nearly 1.5-fold) than the corresponding PCL/Ch scaffolds.

In-vitro biocompatibility studies using human adipose derived stem cells (hAD-MSCs), demonstrated that the presence of only 5 wt% nZnHA in PCL/Ch/nZnHA nanocomposites enhanced hAD-MSCs' attachment compared to PCL/Ch and PCL/Ch/nHA. Finally, hAD-MSCs proliferation occurred at significantly higher rates of 1.5, 1.3 and 1.2 times on PCL/Ch/nZnHA scaffold compared to PCL, PCL/Ch and PCL/Ch/nHA, respectively.

© 2014 Elsevier Ltd. All rights reserved.

1. Introduction

Tissue engineering, as evolved decades ago, combines principles of engineering and life sciences to improve tissue function. This approach allows organs to be grown based on implantation and particularly when autologous undifferentiated cell source is used it eliminates the risk of immunological rejection (Mano & Reis, 2007). One of the important practices in tissue engineering is making a three-dimensional scaffold with appropriate degradation profile. The interconnected pore network of scaffolds provides a suitable micro-environment for cells attachment, proliferation, migration and differentiation (Langer & Vacanti, 1993). Over the last two decades, many methods have been developed for scaffold fabrication including particulate leaching, gas foaming, freeze-drying, solvent casting, phase separation, self-assembly, and electrospinning, with electrospinning showing the greatest promise. Electrospinning has been extensively used, because the nano-sized polymer fibers have advantages, such as very large surface area to volume ratio, flexibility at surface and superior mechanical performance compared to micro-scale fibers (Teo & Ramakrishna, 2006).

Over the last decade, considerable attention has been directed toward the use of hydroxyapatite (HA) in biocomposites. HA, a major inorganic component of natural bone, extensively used as biomedical implant and in bone regeneration due to its bioactivity, and osteoconductivity (Shokrollahi et al., 2014). It displays significant compatibility effect with a large group of synthetic and natural polymers such as polyesters and polysaccharides (Liu et al., 2014; Mekhail, Jahan, & Tabrizian, 2014; Pighinelli & Kucharska, 2013).

On the other hand, the biological HA crystals in vivo, carry many contaminants, e.g., K^+, Mg^{2+}, Na^+, CO_3^{2-} and F^- as partial substitutions which usually reflect dietary history, but can also indicate exposure to environmental hazards, e.g. Pb^{2+} (Narasaraju & Phebe, 1996). These ionic substitutions can alter the properties and in particular osteoconductivity of HA. Webster et al. (2004) have reported a significant increase in osteoblasts adhesion to Zn^{2+} doped HA

* Corresponding author. Tel.: +98 21 48662513; fax: +98 21 44580023.
E-mail addresses: fereshte.may05@gmail.com (F.M. Ghorbani), kaffashi@ut.ac.ir (B. Kaffashi), p.shokrolahi@ippi.ac.ir, pshokrollahi@gmail.com (P. Shokrollahi), seyedjafari@ut.ac.ir (E. Seyedjafari), r.ardeshiry.62@gmail.com (A. Ardeshirylajimi).

http://dx.doi.org/10.1016/j.carbpol.2014.10.071
0144-8617/© 2014 Elsevier Ltd. All rights reserved.

in comparison with undoped HA. Furthermore, Ito, Ojima, Naito, Ichinose, and Tateishi (2000), reported that proliferation of mouse osteoblast-like cells in tricalcium phosphate/HA composite ceramic was enhanced upon Zn^{2+} doped HA. However, HA has not been extensively utilized in tissue engineering applications, because of weak impact properties and inherent brittleness (Kim, Knowles, & Kim, 2004).

To combine the osteoconductivity of HA and good processability of polyesters by blending of synthetic polymers with natural and/or synthetic bioceramics has been considered in bone tissue engineering application. Polycaprolactone (PCL), a semi crystalline polyester, is one of the most commonly applied synthetic polymers in medical applications, particularly, because of its hard and soft tissue compatibility, as well as its approved biodegradability (Woodruff & Hutmacher, 2010). Nevertheless, properties such as weak hydrophilicity, acidic nature of the degradation products, relatively slow degradation profile and neutral charge distribution have restricted its usage (Zhu, Gao, Liu, & Shen, 2002). Recently, chitosan, the product of *N*-deacetylation of chitin, has received much attention for tissue engineering applications, because of its biocompatibility, biodegradability, hydrophilicity and anti-microbial activity (Tsai et al., 2012). Also, a core shell structured PLLA/chitosan nanomat was co-axially electrospun and successfully examined as drug carrier in tissue engineering (Ji & Yang, 2013). However, chitosan suffers from weak mechanical properties in wet state. So, blending of chitosan with PCL, as electrospun nanomats (Schueren et al., 2012, 2013) or electrospun multilayer mats (Lou et al., 2014), has been considered as a strategy to develop new biomaterials that exhibit hybrid properties, which are not obtained by either of these individual polymers.

Despite the publication of numerous reports on PCL/HA and Ch/HA nanocomposite designs and their preparation destined for biomedical applications, there are very few reports on electrospinning of a tri-component PCL/Ch/HA nanocomposite system in biomedical applications in the literature. There are still less publications reported in literature on enhanced bone tissue compatibility using polymer composites containing HA nanoparticles doped with metals such as Mg, Sr, or Zn, with their well known potential in enhancement of osteoconductivity (Fujii et al., 2006; Webster et al., 2004).

In the present study, we have used electrospinning to produce PCL/chitosan/nHA nano composite scaffolds. Composites were prepared using a solution blending technique as was suggested by Schueren et al. (2012), but with different compositions. Also aiming to improve biocompatibility/osteoconductivity, nano HA was partially doped with Zn^{2+} ions.

2. Materials and methods

2.1. Materials

Medium molecular weight chitosan with degree of deacetylation 80–85%, PCL (M_n 70,000–90,000 g mol^{-1}), and zinc nitrate were supplied by Sigma-Aldrich. Formic acid and acetic acid were obtained from Merck Chemicals. All chemicals were used as received unless recommended otherwise.

2.2. Preparation of polymer blends

A solution strategy was adopted in polymer blending. Chitosan was dissolved in a formic acid (70%)/acetic acid (70%), mixed solvent system (volume ratio = 70/30), to yield 3 w/v% solution. PCL was dissolved in formic acid (glacial)/acetic acid (glacial), mixed solvent system (volume ratio = 70/30), to prepare a solution of 3 w/v% concentration. These solutions were then mixed together at appropriate ratios to afford desired blend compositions.

A series of PCL/chitosan blends was prepared while the PCL:chitosan weight ratio was adjusted at 90/10, 80/20, and 50/50, which are referred to as PCL/Ch(10), PCL/Ch(20) and PCL/Ch(50), respectively, hereafter.

2.3. Synthesis of Zn doped HA nanoparticles

HA and Zn-doped HA nanoparticles(nZnHA), were produced according to literature (Webster et al., 2004). Briefly, for HA preparation, to a solution of $Ca(NO_3)_2{\cdot}4H_2O$ (1 M), in double distilled water (DD water), was added diammonium hydrogen phosphate(0.6 M), at room temperature while the pH was carefully adjusted at 11–12 over the addition process. The solution was stirred for 24 h, while nHA precipitated out. The nanoparticles were washed with DD water and centrifuged in triplicate, rinsed and dried for 24 h at 70 °C. The previous recipe was repeated for nZnHA synthesis, except to a Zn^{2+} containing (5 wt%), solution of $Ca(NO_3)_2{\cdot}4H_2O$ (1 M), in DD water, was added diammonium hydrogen phosphate (0.6 M), at room temperature while the pH was carefully adjusted at 11–12 over the addition process. Finally, a work up procedure similar to what mentioned for nHA recovery was followed to obtain nZnHA.

2.4. Composite preparation

nHA (especially synthesized and used for comparative biocompatibility assays) and Zn-doped hydroxyapatite nanoparticles (nZnHA) containing scaffolds were generated by admixing HA nanoparticles (a dispersion of 5 w/v% in formic acid (70%)/acetic acid (70%), solvents volume ratio = 70/30), to the polymer blend solutions. The precisely controlled volumes of the nHA or the nZnHA suspensions were added to PCL/chitosan blend solutions in order to yield final composites with 5 wt% bioceramic content relative to the total polymer mass in all compositions reported here. For example, PCL/Ch(10)/nZnHA nanocomposite indicates that it may have been prepared by addition of appropriate volumes of the above nZnHA suspension to a solution of PCL/chitosan (90/10), to afford a mixture in which the net share of nZnHA in dry state would be 5 wt%.

All solutions were then sonicated for 20 min at room temperature and further homogenized using a homogenizer probe at 7500 rpm for 10 min and stirred at room temperature to achieve homogeneous solutions.

2.5. Composite Characterization

2.5.1. Electrospinning of PCL/chitosan/nHA, and PCL/chitosan/nZnHA nanofibers

The stock solutions were fed into a 10 ml syringe equipped with a needle of 0.7 mm inner diameter. Electrospinning was carried out at room temperature. A flat aluminum plate was kept at predetermined distance (Table 1), from the syringe needle tip for fiber collection. Windows of a stable electrospinning condition for polymer blends and polymer nanocomposites are given in Table 1.

2.5.2. Scanning electron microscopy (SEM)/field emission SEM (FESEM)

To evaluate morphologies of the electrospun nanofibrous scaffolds, SEM (VEGA, TESCAN, Czech Republic) was used. SEM images were acquired at 20 kV after sputtering of a thin gold film on the samples. The nanocomposite scaffolds were also observed using a TESCAN field emission scanning electron microscope (FESEM), equipped with an energy dispersive spectrometer (Oxford), at 12 kV.

Table 1
Optimized electrospinning conditions for PCL/chitosan and PCL/chitosan/nZnHA (5 wt% against total polymer mass) of different compositions.

PCL/Ch blends			
PCL/Ch ratio	90/10	80/20	50/50
Flow rate (ml/h)	0.5	0.5	0.7
Voltage (kV)	15	15	25
Working distance (cm)	12.5	12.5	12.5
Needle diameter (mm)	0.7	0.7	0.7
PCL/Ch/nHA nanocomposites (5 wt% nZnHA)			
PCL/Ch ratio	90/10	80/20	50/50
Flow rate (ml/h)	0.7	0.7	1
Voltage (kV)	20	20	30
Working distance (cm)	12.5	12.5	12.5
Needle diameter (mm)	0.7	0.7	0.7

2.5.3. Energy dispersive X-ray analysis (EDXA)

A FESEM equipped with an EDXA detector was used to determine calcium, phosphorus and zinc contents of the synthesized Zn-doped nanohydroxyapatite particles. EDXA was performed at an acceleration voltage of 20 kV and magnification of 280×.

2.5.4. Atomic force microscopy

AFM was performed in tapping mode on thin films of samples at RT (Dual Scope-DME), using silicon cantilever tips.

2.5.5. XRD analysis

Wide angel X-ray scattering, WAXs, data were obtained using a Siemens D5000 instrument, which was a theta/2theta diffraction instrument operating in reflection geometry using Fe$K\alpha$ radiation, $\lambda = 1.93604$ angstroms, focussed by a Ge crystal primary monochromator.

2.5.6. Attenuated total reflectance Fourier transform infrared (ATR FTIR) spectroscopy

ATR FTIR spectra were collected using a Bruker, Equinox55 spectrometer equipped with Specac Silver Gate single reflection ATR accessory (ZnSe crystal).

2.5.7. Mechanical properties

Tensile tests were carried out on a STM 20 (Santam, Iran) universal testing machine at room temperature. A 200 N load-cell was used for the test at a crosshead speed of 1 mm min^{-1}. Bar shaped tensile specimens ($30 \times 5 \times 1$ mm^3) were cut from the scaffolds sheets. The grip to grip distance was 20 mm, and at least four measurements were conducted for each sample.

2.5.8. Degree of hydration

Samples of PCL, PCL/Ch (10), PCL/Ch (10)/nHA, and PCL/Ch (10)/nZnHA, as bars (10–20 mg), were incubated in PBS(2 ml sample^{-1}) for 48 h at 37 °C while shaken at 60 rpm. 3 samples of each composition were used to measure the degree of hydration after that; the samples were wiped and weighed with an accuracy of ±0.1 mg. Degree of hydration (W_U%) was calculated using the following equation:

$$W_U = \left(\frac{(W_a - W_0)}{W_0}\right) 100\%$$

where W_a and W_d indicating the wet and the dry weights of samples, respectively.

2.5.9. Protein adsorption

The scaffold adsorption of model proteins were evaluated according to a protocol reported with Laschke et al. (2010). In brief, after sterilization, the scaffolds ($n = 9$; size $3 \times 3 \times 1$ mm^3) were incubated in phosphate-buffered saline (PBS; 10 mM, pH 7.4) containing fetal bovine serum (FBS, for which bovine serum albumin (BSA, holding an isoelectric pH of 4.7 at 25 °C), was the major component, 1 vol%) at 37 °C for 60 min. The initial concentrations of the protein solutions were measured by a BioTek microplate reader (USA) at 530 nm. The nanofibrous scaffolds were washed twice with 10 mM PBS (at the end of the FBS incubation period), and incubated in 500 μl of PBS containing 2.0 wt% sodium dodecylsulfate (SDS) for 20 h to detach the adsorbed proteins on the surfaces of the nanofibrous scaffolds. The total protein concentration values in the PBS solution containing 2.0 wt% SDS were quantified with a BioTek microplate reader (USA) at 530 nm of absorbance by means of a commercial protein assay kit (BCA; Pierce, Rockford, IL, USA) following the manufacturing instructions. The average measurements of adsorbed proteins are reported in μg of proteins per mm^3 of scaffold measured from a BSA calibration in 2.0 wt% SDS in 10 mM PBS.

2.6. Cell culture

2.6.1. Cell seeding

Prior to cell seeding, circular scaffolds were immersed in the following solutions: (1) 70% ethanol (1 h) for sterilization (Cooper, Bhattarai, & Zhang, 2011), (2) penicillin, streptomycin, and amphotericin B to prevent bacterial infection and yeast growth (Shearer & Ellis, 2006), and (3) culture medium to enhance cell attachment after seeding. Human adipose tissue derived stem cells (hAD-MSCs) were used for cell seeding. They were isolated from human adipose tissue, cultured and maintained in Dulbecco's modified Eagle's medium supplemented with 10% fetal bovine serum and a 1% antibiotic (10,000 U penicillin). hAD-MSCs were trypsinized and seeded on to the circular scaffolds with an initial cell density of 10^4 cm^{-1} and incubated in the culture medium.

2.6.2. Cell morphology

Cell morphology on the scaffolds was evaluated by scanning electron microscopy. The cell-loaded scaffolds were rinsed with PBS after 3 days of cell seeding and fixed in glutaraldehyde (2.5%) for 1 h. For dehydration, the scaffolds were placed in a series of gradient alcohol concentration and then dried.

2.6.3. MTT assay

The proliferation rates of hAD-MSCs on scaffolds were evaluated via MTT assay. Sterilized nanofibrous membranes were placed in a 24-well culture plate, seeded with a cell density of 4×10^3 cells per cm^2, and incubated at 37 °C and 5% CO_2. After 24, 48 and 72 h, 4 and 5 days of cell seeding, 50 μl of MTT solution (5 mg ml^{-1} in DMEM) was added to each well ($n = 4$). For conversion of MTT to formazan crystals by mitochondrial dehydrogenases of living cells, the plate was incubated at 37 °C for 4 h. For dissolution of the dark-blue intracellular formazan, the supernatant was removed and a definite amount of dimethyl sulfoxide (DMSO), as solvent, was added. The optical density was read at a wavelength of 570 nm in a BioTek micro-plate reader (USA). The same procedure was performed for cells cultured on tissue culture polystyrene (TCPS) as control.

2.7. Statistical analysis

Statistical analysis was performed using one-way ANOVA. All results are reported as the mean value 6 of standard deviation. Differences were considered statistically significant at $p < 0.05$.

3. Results

3.1. Characterization of Zn-doped hydroxyapatite nanoparticles

The synthesized bioceramic nanoparticles (namely nZnHA), were characterized by SEM, X-ray diffraction and energy disperse X-ray analysis(EDXA). Fig. 1A shows the SEM image of nZnHA synthesized in this study and Fig. 1B shows X-ray diffraction pattern of the Zn-doped HA particles. The existence of 2θ peaks at 23.5°, 26° and 32.5° corresponding to the diffraction planes (2 1 1), (0 0 2) and (3 0 0) of the HA crystallites, respectively, confirms formation of HA (Nikpour, Rabiee, & Jahanshahi, 2012). A slight difference is observed between the XRD patterns of HA and nZnHA, which is in perfect agreement with those previously reported by Fujii et al. (2006), for similar studies. EDXA pattern of the Zn-doped HA is given in Fig. 1C and the presence of Zinc in the HA structure is evident in the EDXA spectrum (Fig. 1C, about 5 wt% by EDXA analysis).

3.2. Morphology of PCL/Ch and PCL/Ch/nZnHA nanofibers

Optimization of the electrospinning parameters for fabrication of PCL/Ch and PCL/Ch/nZnHA fibers was required because most current processes use fiber-forming additives such as poly(ethylene oxide)(PEO) or poly(vinyl alchohol)(PVA) to improve the spinnability of natural polymers (Klossner et al., 2008). However, in the current study, to avoid any traces of unwanted components in the final product, we tried to obtain fibers without using additives. Initial optimization included systematically adjusting the solution concentration, flow rate, working distance and voltage of the electrospinning condition to yield bead-free electrospun nanofibers that to become continuous and uniform in shape. Based on previous studies, an optimal total mass concentration of 3 w/v% was selected for the chitosan and the polycaprolactone solutions (Gholipour, Bahrami, & Nouri, 2009). To determine the electrospinning region of PCL/Ch and PCL/Ch/nZnHA nanofibers, solutions containing different polymer ratios (10/90–20/80–50/50) were attempted to electrospin, for which the stable electrospinning conditions are reflected in Table 1.

Electrospinning of the pure chitosan solution resulted in formation of polymer droplets on the collector without any sign of nanofiber formation. A possible explanation for this observation could be due to the inability of jet formation during electrospinning of a high bulk viscosity and pseudoplastic structure of the chitosan solution. Addition of chitosan to PCL solutions led to a significant increase in the solution viscosity. In addition to the viscosity, chitosan is a polyelectrolyte that exists in charged form in solution. Strong repulsive forces between ionogenic groups within the polyelectrolyte backbone impede the formation of continuous fibers. However, continuous fibers with no beads are achieved even at PCL/chitosan blend of 50/50 weight ratio, by aptly changing the electrospinning parameters (Table 1). Also, addition of HA nanoparticles into the blended polymer solutions led to an increase in viscosity, and thus the electrospinning parameters needed readjustment for each composite sample. As it can be seen in Fig. 2, the mean diameter of the obtained nanofibers varies in the range of 138–164 nm for PCL/Ch (10) and 210–90 nm for the PCL/Ch (10)/nZnHA electrospun scaffolds.

Fig. 2A–F show FESEM images of the electrospun PCL/chitosan nanofibers, which reveal the well-oriented and bead-free nanofibers with smooth surfaces and uniform diameters along their lengths. The nanofibers grew thicker as the content of chitosan decreased.

The reason for obtaining a reduced diameter in spite of having higher solution viscosity in blends of higher chitosan content was due to the charge density in the ejected jet, which imposed higher elongation forces leading to thinner fiber formation, which was in agreement with previously published data (Klossner et al., 2008).

In contrast to the smooth surfaces of PCL/chitosan nanofibers (Fig. 2). PCL/chitosan/nZnHA fibers contained nanoparticles dispersed on the surface (Fig. 2G–L, circled area), which resulted in surfaces of higher roughness.

HA did not affect electrical conductivity of the electrospinning solutions, therefore, the obtained morphology was the same as that of PCL/chitosan, however, fiber diameter increased dramatically (Fig. 2G–L). These behaviors are particularly interesting because the whole structure mimics the mineral crystals of the natural hard tissue and have been shown to induce a significant increase in specific protein absorption and cell adhesion, compared to their micro-size counterparts (Balasundaram, Sato, & Webster, 2006; Kokubo et al., 2004).

3.3. Characterization of PCL/chitosan/nHA nanofibers

Two independent approaches, energy dispersive Xray analysis (EDXA) and attenuated total reflectance Fourier transform infrared (ATR-FTIR) spectroscopy, were employed to further characterize the PCL/chitosan/nHA. EDXA was used to determine the elemental composition of the individual nanofibers. PCL/chitosan/nHA scaffolds showed large peaks for carbon and oxygen and a small peak for nitrogen, indicating three of the major components of chitosan and PCL (Fig. 3A). EDXA spectrum of PCL/chitosan/nHA, bearing 5 wt% HA in the composition, showed small amounts of calcium and phosphorus (Fig. 3A). The elemental dispersion maps, acquired by EDXA, were evidence of a uniform distribution of calcium and phosphorus (Fig. 3B) on the surface of nanofibers.

Our studies were then extended to morphology of the PCL/Ch/nZnHA nanocomposites using AFM. AFM observation (Fig. 3C–E), revealed that nZnHA nanoparticles were mainly present in PCL phase (continuous phase). Composition-dependent phase structure of the nanocomposites was studied in great details and the results will be reported in a separate article. Fig. 3E depicts that surface roughness is influenced by presence of nZnHA nanoparticles.

Fig. 4A presents ATR–FTIR spectra of PCL, chitosan and hydroxyapatite. Several characteristic bands located at 2940, 1725 and 1245 cm^{-1} are assigned to ester groups of PCL (Wu et al., 2008). Two typical bands at 1598 and 1640 cm^{-1} for amino group of chitosan are also observed. The characteristic peak of pure nHA at 3500 cm^{-1} corresponds to —OH group and the band at 1110 cm^{-1} originates from PO_4^{3-} group. The IR spectra of PCL/Ch(10) and PCL/Ch(10)/nHA are presented in Fig. 4A. From the spectrum of PCL/Ch(10)/nHA (Fig. 4B and C), one concludes that the characteristic band of amino group in chitosan at 1638 cm^{-1} and ester group in PCL at 1238 are disappeared, as an indication of possible electronic interactions and hydrogen bands formation between the PO_4^{3-} group of nHA and NH_3^+ and carboxyl groups of chitosan and PCL, respectively (Bhattarai et al., 2004. On the other hand, the characteristic band of nHA became less intense and shifted to smaller wavenumbers (from 1110 cm^{-1} to 1091 cm^{-1}) as compared with that of pure nHA, also implying that there was a possibility of electronic interaction between the polymers and nHA. Therefore, based on the data extracted from FT IR spectra, we speculate that there are possible physical interactions (electronic attractions and hydrogen bonding) between nHA, on the one hand, and PCL and chitosan, on the other hand.

3.4. Mechanical properties of PCL/chitosan/nZnHA nanofibers

The effect of nHA and nZnHA on the mechanical properties of PCL/Ch(10) scaffold was tested next. Based on the data extracted from stress–strain curves (Fig. 5) generated for the electrospun

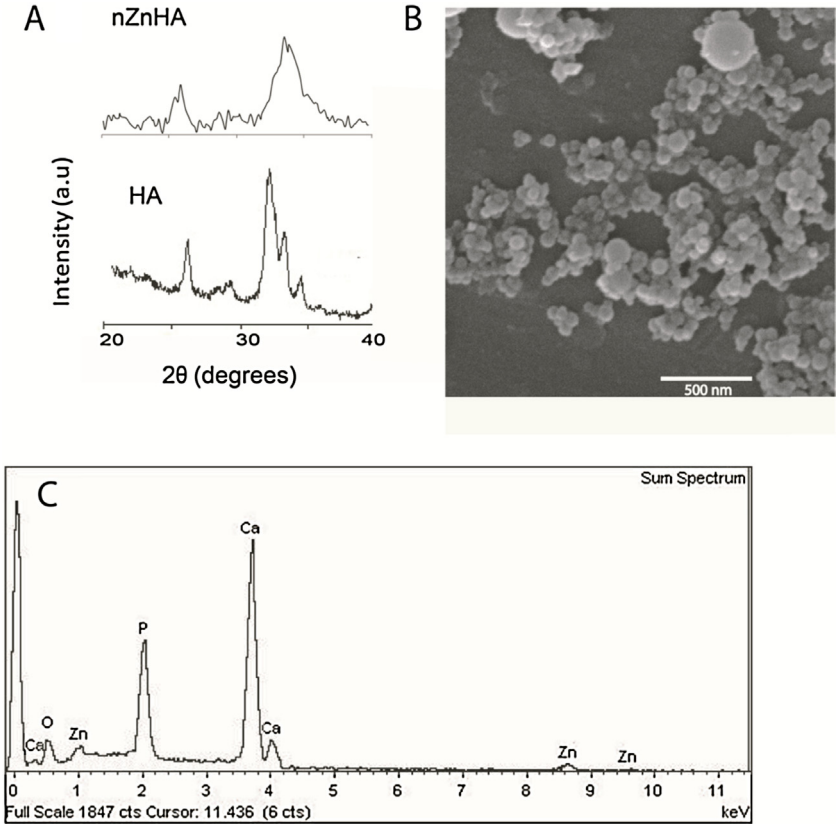

Fig. 1. (A) X-ray diffraction pattern, (B) SEM image and (C) energy dispersive X-ray analysis of the synthesized Zn-doped hydroxyapatite (C_{Zn} is about 5 wt%, Ca/P:1.7, Ca + Zn/P:1.8).

fibrous scaffolds, break stress, elongation-at-break and Young's modulus could be calculated. The tensile property of PCL/Ch(10) was significantly enhanced with addition of HA; the break stress was increased from 11.5 to 19.5 MPa. At the same time, elongation-at-break decreased to 195% (from about 300% recorded for the neat blend) for the PCL/Ch(10)/nHA, However, reportedly, this extent of elongation is enough for bone regeneration (Li, Li, & Jiang, 2012). Furthermore, the Young's modulus of the scaffold increased from 3.5 MPa for PCL/Ch(10) to 11.2 MPa for PCL/Ch(10)/nHA, which was enough to prevent scaffold from deformation. It may be noted that a there was no significant difference observed between the mechanical properties of the composite scaffolds PCL/Ch/nHA and PCL/Ch/nZnHA. These results demonstrate that composite preparation with HA/ZnHA played a great role to enhance the mechanical properties of the fibrous scaffold.

3.5. Biocompatibility of the scaffolds

Success of tissue engineering strategy relies on balanced adjustment of the interplay between cells, regulatory signals, and the biomaterials (scaffolds, hydrogels, etc.), used to deliver this, so called, tissue engineering triad. The osteoconductive properties of calcium phosphates, in general, and hydroxyapatite in particular (as the most commonly used bioceramic), support tissue ingrowth, osteoprogenitor cell growth, and new bone tissue formation through supporting the attachment, proliferation, and differentiation of bone cells. This ability mainly originates from the ability to Ca^{2+} and P ions exchange with extracellular matrix. Based on recent reports, the structural or chemical composition of CaP ceramics can be modified. This includes inclusion of metal ions in the crystal structure of hydroxyapatite (Guarino et al., 2014; Murphy, O'Brien, Little, & Schindeler, 2013). Recently, the effect of Zn^{2+} as a signaling factor on osteogenesis stimulation/bone remodeling has been studied in elaboration, using different bioceramics including hydroxyapatite, β-tricalcium phosphate and bioglass as model compounds (Haimi et al., 2009; Roy, Fielding, Bandyopadhyay, & Bose, 2013). For example, it has been shown that a hydroxyapatite/Zn doped TCP bone cement containing about 0.7% zinc caused a significant increase in human osteoblastic cells proliferation. The same cement with two folds of Zn, on the other hand, was found cytotoxic to human osteoblasts (Ishikawa et al., 2002). Haimi et al. (2009), have reported that the degradation rate of bioglass was reduced upon doping excess amounts of Zn and that this had been translated to lower human adipose stem cells proliferation and osteogenesis (Haimi et al., 2009). On the other hand, oxidative stress kind of damage of human MG-63 osteoblasts was reported in presence of bioactive glass, Hench's 45S5, due to fast Zn release. An inhibitory effect on osteoclasts formation has also been reported for Zinc, in vitro (Aina et al., 2007; Ren, Xin, Ge, & Leng, 2009). All these data highlight the importance of designing Zn containing bioceramics of balanced Zn concentration to avoid toxic effects. Therefore, Zn-doped HA, having a Zn concentration of about 5 wt% was synthesized and used in this study.

3.6. Protein adsorption

It is well known that protein adsorption has a determining influence on the biological properties of calcium phosphate containing bioceramics. Therefore, protein adsorption on PCL, PCL/Ch(10), PCL/Ch(10)/nHA and PCL/Ch(10)/nZnHA samples were measured and compared in this study. From the data given in Fig. 6, it can be

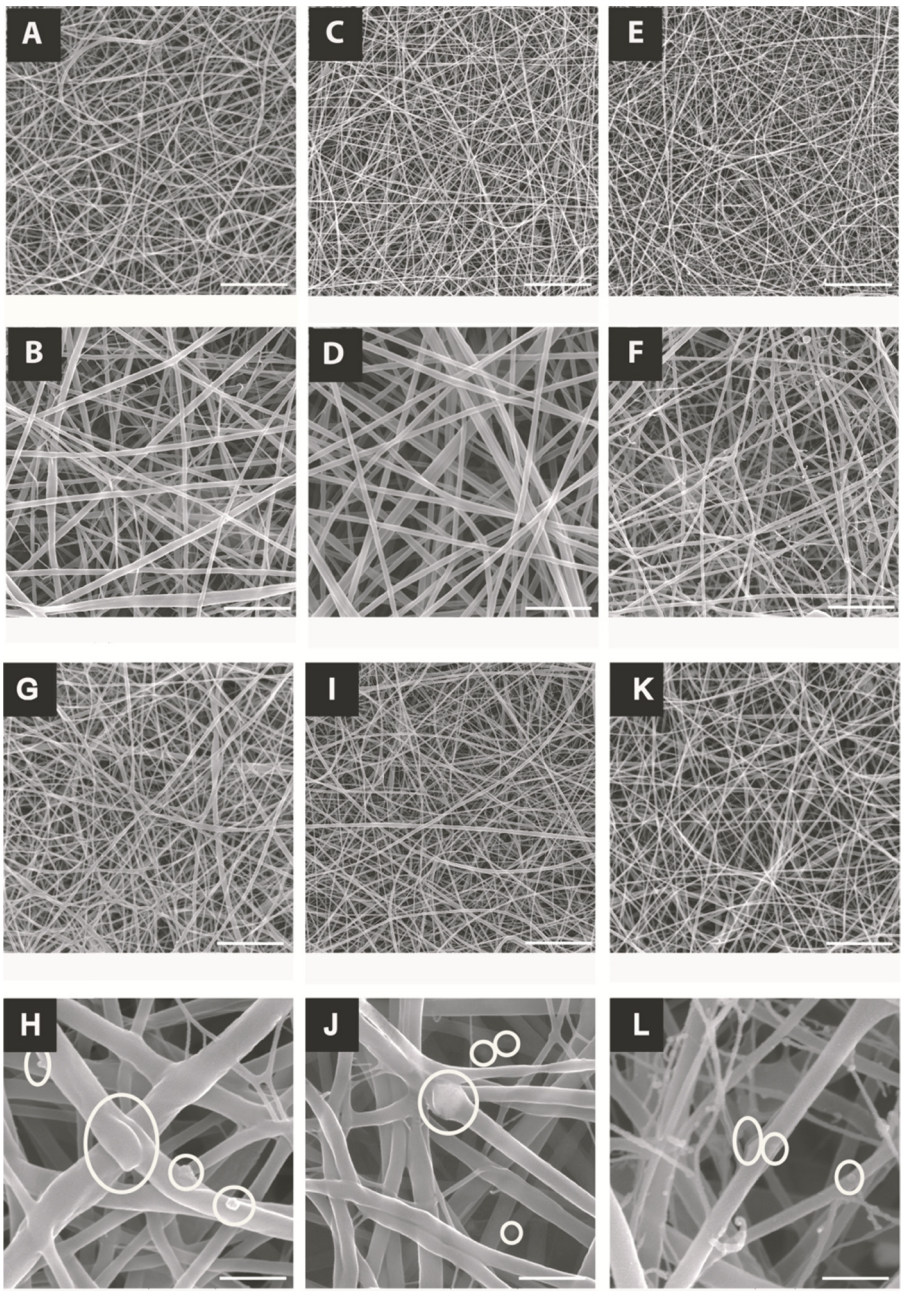

Fig. 2. (A–F) Representative FESEM images of electrospun blend scaffolds; (A/B) PCL/Ch(10), (C/D) PCL/Ch(20), and (E/F) PCL/Ch(50). (B and D) and (F) give a closer view to the structures given in (A, C and E), scale bars: (A and C) and F 5 μm & (B and D) and (F) 1 μm. (G–L) representative FESEM images of electrospun nanocomposite scaffolds; (G/H) PCL/Ch(10)/nZnHA, (I/J) CL/Ch(20)/nZnHA, and (K/L) PCL/Ch(50)/nZnHA. (H, J and L) give a closer view to the structures given in (G, I and K). Scale bars: (G, I and K) 5 μm & (H and J and L) 500 nm.

concluded that all types of the scaffolds adsorb FBS on their surfaces, but the most significantly absorbed protein was observed on PCL/chitosan/nZnHA and PCL/chitosan/nHA nanofibrous scaffolds. However, PCL/chitosan also adsorbed a significantly larger amount of protein than PCL nanofibers. A relatively large number of parameters have been considered for their controlling role in protein adsorption on bioceramic containing polymer based (nano-) composites. Among them different material properties(such as chemical composition and surface properties including topography and hydrophilicity), different protein properties (e.g., size, charge, structure stability and unfolding rate) and environment (such as pH of the protein solution), have been studied in great details (Dee, Puleo, & Bizio, 2003). Since FBS contains a number of different proteins, it has not been possible to extract information on environmental parameters and charge, structure stability and unfolding rate of the adsorbed proteins on the protein adsorption in the present study. Increased hydrophilicity of the blend and the nanocomposite scaffolds (Table 2), compared to pure PCL is

Table 2
Relative degree of hydration of fibrous scaffolds.

Sample	Hydration (%)
PCL	20 ± 0.1
PCL/Ch(10)	40 ± 0.1
PCL/Ch(10)/nHA	35 ± 0.4
PCL/Ch(10)/nZnHA	35 ± 0.2

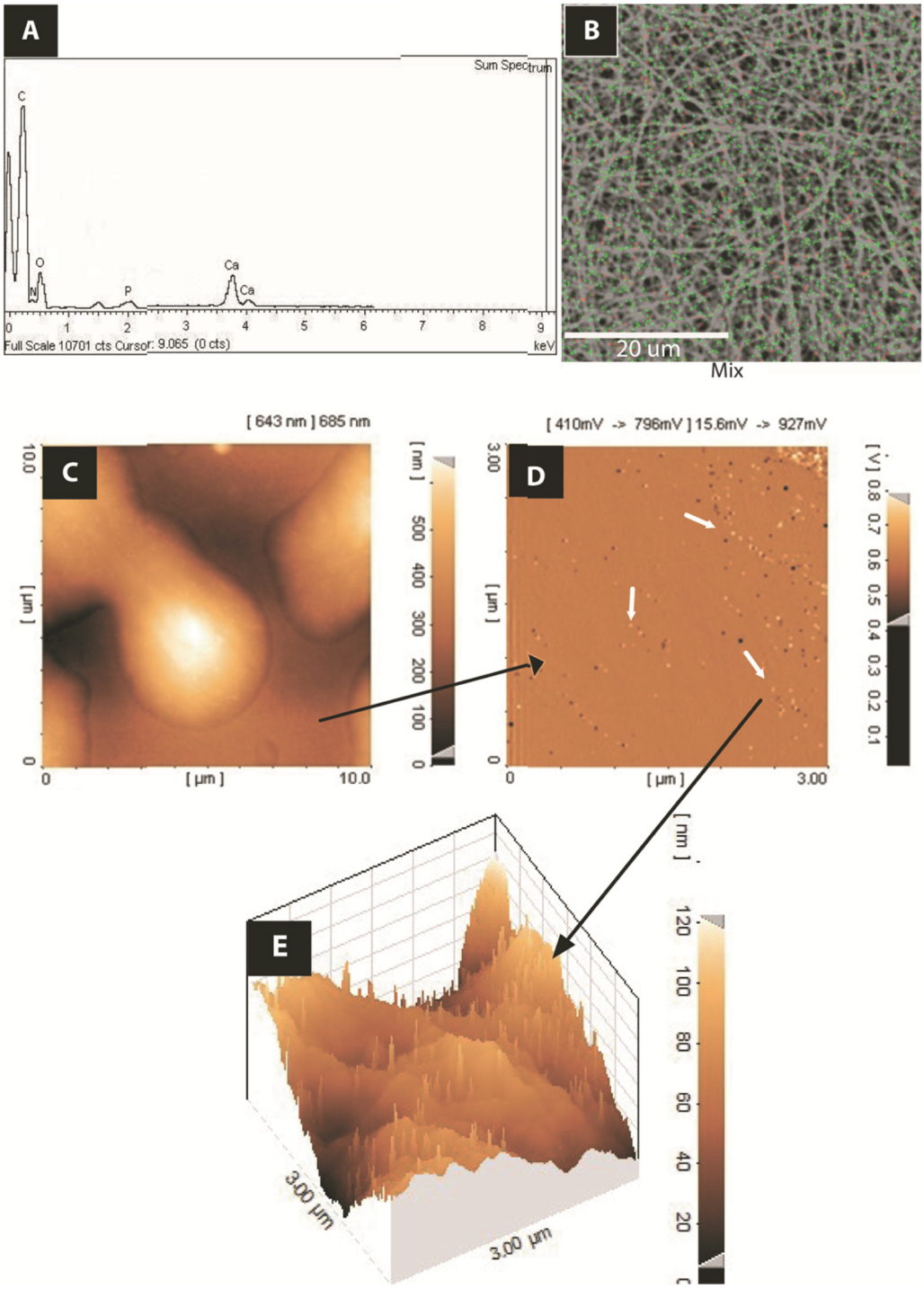

Fig. 3. (A) Energy dispersive Xray analysis of PCL/Ch(10)/nHA biocomposite nanofibers. EDXA spectrum shows peaks of calcium and phosphorous. (B) Dot-analysis represents the elemental distribution mapping of calcium (green dots) and phosphorous (red dots) within the nHA-containing nanofibers. (C, D and E) Effect of presence of nHA on surface roughness was also studied with AFM. (For interpretation of the references to color in this figure legend, the reader is referred to the web version of this article.)

considered as the parameter, which may play a role in enhancement of the protein adsorption. Besides that, roughness, porosity and pore size have pronounced effect on protein adsorption capacity of polymer/bioceramic composite scaffolds. Increase in any of these features may result in enhanced specific surface area and is translated into superior protein adsorption. In Fig. 3E (AFM observation), a surface of higher roughness is expected for the nanocomposite electrospun scaffolds, which justifies the higher protein adsorption. The PCL/Ch(10)/nZnHA composite, showed the highest level of protein adsorption among the samples studied. Since FBS, as the protein source used, is a rich source of different proteins, cell adhesion and proliferation studies were also carried out to define whether the protein adsorption could adequately support cell activities on our PCL/Ch, PCL/Ch/HA and PCL/Ch/nZnHA nanofibrous scaffolds.

3.7. Cell adhesion and proliferation

Cell response of the nanofibrous scaffolds was investigated via SEM observation and MTT assay. Scanning electron micrographs

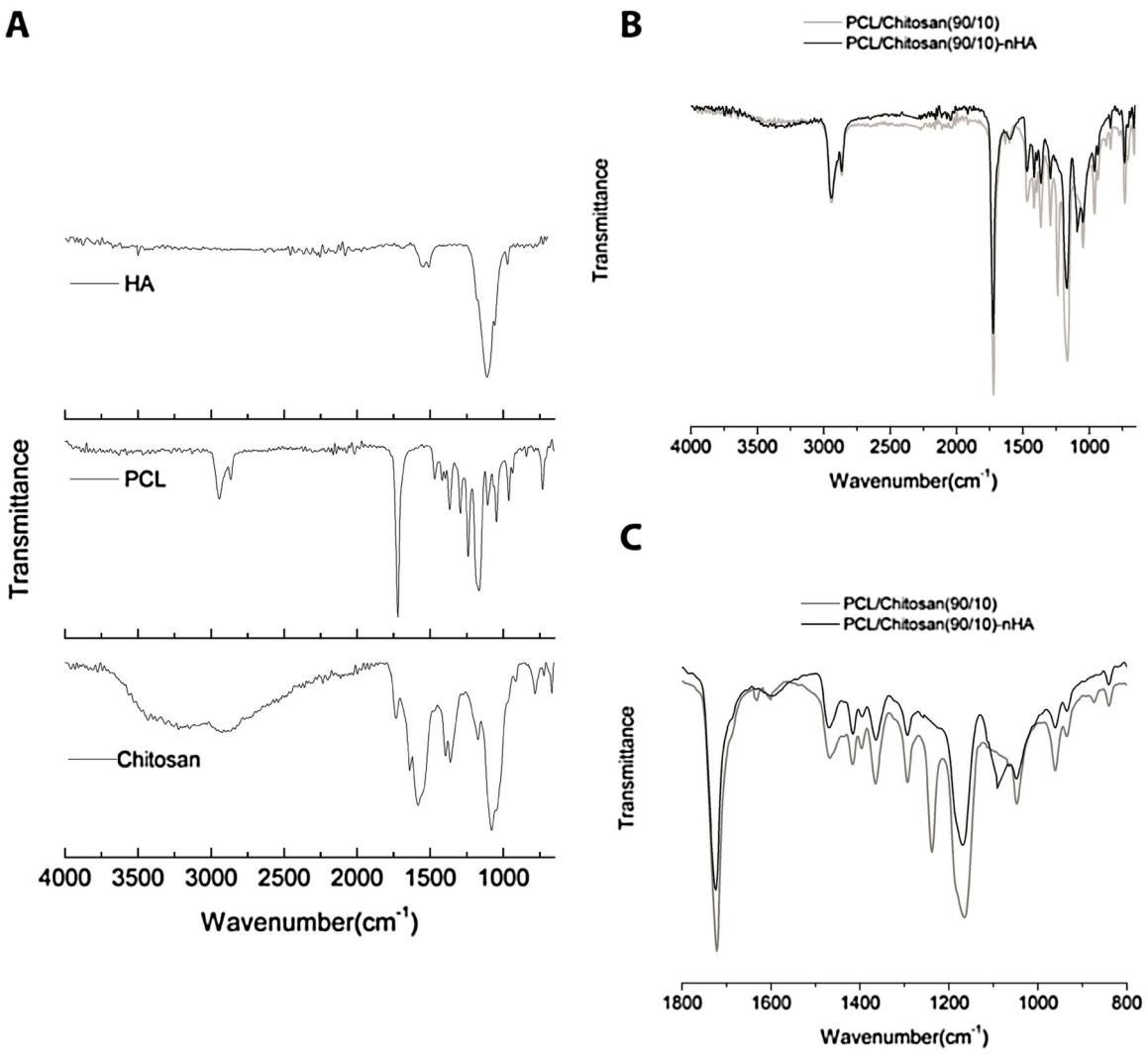

Fig. 4. ATR-FTIR spectra of (A) pure PCL, chitosan and hydroxyapatite. (B) PCL/Ch(10), PCL/Ch(10)/nHA and (C) a closer view to the spectra given in (B) (nHA, 5 wt%).

of the nanofibrous scaffolds after three days of cell culture is shown in Fig. 6. Proliferation rates and viability of hAD-MSCs cultured on PCL, PCL/Ch(10), PCL/Ch(10)/nHA and PCL/Ch(10)/nZnHA nanofibrous scaffolds were evaluated by MTT assay (Fig. 6). The results demonstrate that by five days post-seeding the highest cellularity was achieved in PCL/Ch(10)/nZnHA compared to other groups.

Cell adhesion rate of scaffolds was evaluated via MTT assay 5 h after seeding, and the results are summarized in Fig. 6(up); the most significant number of cells adhered to surface was

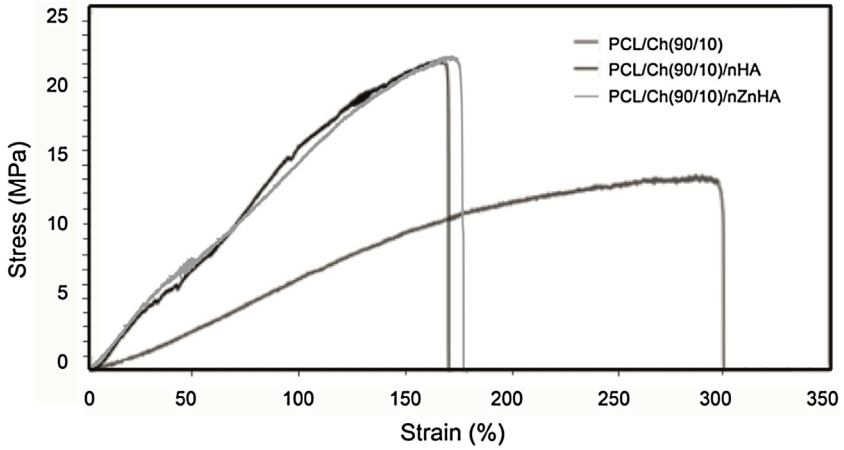

Fig. 5. Stress–strain curves of the nanofibrous PCL/chitosan (90/10) scaffold in comparison with nanofibrous PCL/Ch(90/10)/nHA (5 wt% related to total polymer mass) and nanofibrous PCL/Ch(90/10)/nZnHA (5 wt% related to total polymer mass) scaffolds.

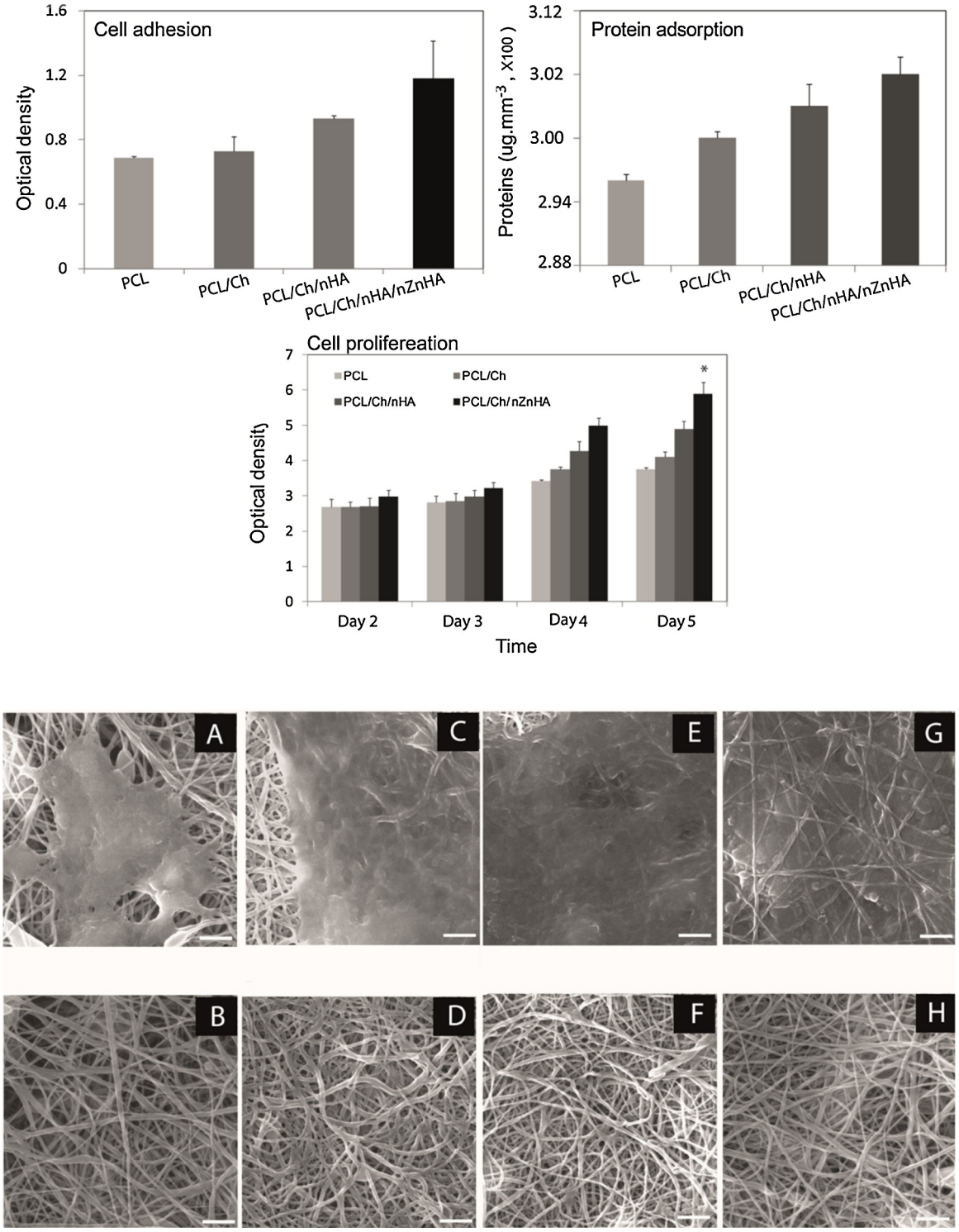

Fig. 6. UP: Results of protein adsorption (5 h post seeding), cell adhesion (MTT assay, 5 h post seeding) and cell proliferation (MTT assay, a final culture period of 5 days), on PCL, PCL/Ch(10), PCL/Ch(10)/nHA, and PCL/Ch(10)/nZnHA. * Change is significant $p < 0.05$, $n = 3$, relative to PCL/Ch/nHA scaffold. Down: SEM observation of hAD-MSCs coverage on PCL(A), PCL/Ch(10)(C), PCL/Ch(10)/nHA(E) and PCL/Ch(10)/nZnHA(G), fibrous scaffolds, scale bars represent 2 μm, for the sake of comparison the scaffolds were observed with SEM at the same magnification before cell seeding (B, D, F and H).

observed for PCL/Ch(10)/nZnHA nanofibrous scaffold. However, PCL/Ch(10)/nHA also contained significantly more cells than PCL and PCL/Ch(10) scaffolds.

Mechanism of osteoblast-like cells adhesion onto metal ion containing bioceramics has been recently studied and reported by Hoppe, Guldal, and Boccaccini (2011) in great details.

Zn^{2+} ions are well known for anti-inflammatory/antibacterial (Kumar et al., 2012) effect accompanied by stimulating bone formation in vitro, which is initiated by protein synthesis in osteoblast-like cells. Zn^{2+} ions also, reportedly increase ATPase activity and regulate transcription of osteoblastic differentiation genes such as collagen, osteopontin and osteocalcin

(Hoppe et al., 2011; Horiuchi et al., 2014). The MTT assay results in this study clearly have shown that synergistic effect of blending with chitosan (as a natural polymer), composite preparation with HA and particularly, Zn doping at small quantity of about 5% in a nanofibrous scaffold morphology could result in remarkable enhancement of hAD-MSCs proliferation only after 5 days culture.

4. Conclusion

A natural biodegradable polysaccharide, chitosan, and a FDA approved synthetic biodegradable polymer, poly(ε-caprolactone), were blended with non-stoichiometric zinc-doped hydroxyapatite nanoparticles(nZnHA) using a mixed formic acid/acetic acid solvent system to electrospin nanofibrous scaffolds. The average fiber diameter was increased from a minimum of about 136 nm, measured for PCL/Ch(50), to about 210 nm recorded for the same blend containing nZnHA (5 wt% of total polymer content). Blending of PCL with chitosan resulted in better hydrophilicity (a doubled hydration for PCL/Ch(10), compared to pure PCL), however, hydration value decreased slightly when nHA (5 wt%) was added into the blend. PCL/Ch(10)/nHA, had higher elastic modulus (about 3-fold) and tensile strength (nearly 1.5-fold) than the corresponding PCL/Ch scaffold. AFM study showed that nHA component led to a higher fiber surface roughness. Also, the analysis by SEM and EDX analyses confirmed uniform distribution of nZnHA in the composite nanofibers. PCL/Ch, PCL/Ch/nHA and PCL/Ch/nZnHA scaffolds supported adhesion and proliferation of adipose derived mesenchymal stem cells (hAD-MSCs). hAD-MSCs proliferated on different scaffolds at a rate order of CL/Ch(10)/nZnHA > PCL/Ch(10)/nHA > PCL/Ch(10) > PCL of five days post culture.

The MTT assay result in this study clearly showed that Zn^{2+} ions also encouraged hAD-MSCs proliferation. Synergistic effect of blending with chitosan (as a natural polymer), composite preparation with HA and Zn doping at small quantity of about 5%, in a nanofibrous scaffold morphology could result in significant enhancement of hAD-MSCs proliferation. Since such scaffolds facilitated attachment and proliferation of hAD-MS cells, we may recommend that they are promising candidates for bone tissue engineering. Further studies are ongoing to monitor the effect of this composite on hAD-MSCs proliferation/differentiation in vitro/in vivo as a function of nHAZn content.

References

Aina, V., et al. (2007). Cytotoxicity of zinc-containing bioactive glasses in contact with human osteoblasts. *Chemico-Biological Interactions*, *167*, 207–218.

Balasundaram, G., Sato, M., & Webster, T. J. (2006). Using hydroxyapatite nanoparticles and decreased crystallinity to promote osteoblast adhesion similar to functionalizing with RGD. *Biomaterials*, *27*, 2798–2805.

Bhattarai, S. R., Bhattarai, N., et al. (2004). Novel biodegradable electrospun membrane: Scaffold for tissue engineering. *Biomaterials*, *25*, 2595–2602.

Cooper, A., Bhattarai, N., & Zhang, M. (2011). Fabrication and cellular compatibility of aligned chitosan–PCL fibers for nerve tissue regeneration. *Carbohydrate Polymers*, *85*, 149–156.

Dee, K. C., Puleo, D. A., & Bizios, R. (2003). *Protein–surface interactions, an introduction to tissue–biomaterial interactions*. Hoboken, New Jersey: John Wiley & Sons, Inc.

Fujii, E., et al. (2006). Selective protein adsorption property and characterization of nano-crystalline zinc-containing hydroxyapatite. *Acta Biomaterialia*, *2006*, 69–74.

Gholipour, A., Bahrami, S. H., & Nouri, M. (2009). Chitosan–poly(vinyl alcohol) blend nanofibers: Morphology, biological and antimicrobial properties. *E-polymers*, *133*, 1–12.

Guarino, V., et al. (2014). MgCHA particles dispersion in porous PCL scaffolds: in vitro mineralization and in vivo bone formation. *Journal of Tissue Engineering and Regenerative Medicine*, *8*, 291–303.

Haimi, S., et al. (2009). Characterization of zinc-releasing three-dimensional bioactive glass scaffolds and their effect on human adipose stem cell proliferation and osteogenic differentiation. *Acta Biomaterialia*, *5*, 3122–3131.

Hoppe, A., Guldal, N., & Boccaccini, A. (2011). A review of the biological response to ionic dissolution products from bioactive glasses and glass-ceramics. *Biomaterials*, *32*, 2757–2774.

Horiuchi, S., Hiasa, M., et al. (2014). Fabrications of zinc-releasing biocement combining zinc calcium phosphate to calcium phosphate cement. *Journal of Mechanical Behavior of Biomedical Materials*, *29*, 151–160.

Ishikawa, K., Miyamoto, Y., et al. (2002). Fabrication of Zn containing apatite cement and its initial evaluation using human osteoblastic cells. *Biomaterials*, *23*, 423–428.

Ito, A., Ojima, K., Naito, H., Ichinose, N., & Tateishi, T. (2000). Preparation, solubility, and cytocompatibility of zinc-releasing calcium phosphate ceramics. *Journal of Biomedical Materials Research*, *50*, 178–183.

Kim, H. W., Knowles, J. C., & Kim, H. E. (2004). Hydroxyapatite/poly(ε-caprolactone) composite coatings on hydroxyapatite porous bone scaffold for drug delivery. *Biomaterials*, *25*, 1279–1287.

Ji, X., & Yang, W. (2013). Coaxially electrospun core/shell structured poly(L-lactide) acid/chitosan nanofibers for potential drug carrier in tissue engineering. *Journal of Biomedical Nanotechnology*, *9*, 1672–1678.

Klossner, R. R., Queen, H. A., et al. (2008). Correlation of chitosan's rheological properties and its ability to electrospin. *Biomacromolecules*, *10*, 2947–2953.

Kokubo, T., Hanakawa, M., et al. (2004). Apatite formation on non-woven fabric of carboxymethylated chitin in SBF. *Biomaterials*, *25*, 4485–4488.

Kumar, P. T., Lakshmanan, V. K., et al. (2012). Synthesis and biological evaluation of chitin hydrogel/nano ZnO composite bandage as antibacterial wound dressing. *Journal of Biomedical Nanotechnology*, *8*, 891–900.

Langer, R., & Vacanti, J. P. (1993). Tissue engineering. *Science*, *260*, 920–926.

Laschke, M. W., et al. (2010). In vitro and in vivo evaluation of a novel nanosize hydroxyapatite particles/poly(ester-urethane) composite scaffold for bone tissue engineering. *Acta Biomaterialia*, *6*, 2020–2027.

Li, L., Li, G., Jiang, J., et al. (2012). Electrospun fibrous scaffold of hydroxyapatite/poly(ε-caprolactone) for bone regeneration. *Journal of Materials Science: Materials in Medicine*, *23*, 547–554.

Liu, X., Chen, Y., et al. (2014). A novel thermo-sensitive hydrogel based on thiolated chitosan/hydroxyapatite/beta-glycerophosphate. *Carbohydrate Polymers*, *110*, 62–69.

Lou, T., Leung, M., et al. (2014). Bi-layer scaffold of chitosan/PCL-nanofibrous mat and PLLA-microporous disc for skin tissue engineering. *Journal of Biomedical Nanotechnology*, *10*, 1105–1113.

Mano, J. F., & Reis, R. L. (2007). Osteochondral defects: Present situation and tissue engineering approaches. *Tissue Engineering and Regenerative Medicine*, *1*, 261–273.

Mekhail, M., Jahan, K., & Tabrizian, M. (2014). Genipin-crosslinked chitosan/poly-l-lysine gels promote fibroblast adhesion and proliferation. *Carbohydrate Polymers*, *110*, 91–98.

Murphy, C. M., O'Brien, F. J., Little, D. G., & Schindeler, A. (2013). Cell-scaffold interactions in the bone tissue engineering triad. *European Cellular Materials*, *26*, 120–132.

Narasaraju, T. S. B., & Phebe, D. E. (1996). Review: Some physico-chemical aspects of hydroxylapatite. *Journal of Mater Science*, *31*, 1–21.

Nikpour, M. R., Rabiee, S. M., & Jahanshahi, M. (2012). Synthesis and characterization of hydroxyapatite/chitosan nanocomposite materials for medical engineering applications. *Composites, B: Engineering*, *43*, 1881–1886.

Pighinelli, L., & Kucharska, M. (2013). Chitosan–hydroxyapatite composites. *Carbohydrate Polymers*, *93*, 256–262.

Ren, F., Xin, R., Ge, X., & Leng, Y. (2009). Characterization and structural analysis of zinc-substituted hydroxyapatites. *Acta Biomaterialia*, *5*, 3141–3149.

Roy, M., Fielding, G., Bandyopadhyay, A., & Bose, S. (2013). Effects of zinc and strontium substitution in tricalcium phosphate on osteoclast differentiation and resorption. *Biomaterials Science*, *1*, 74–82.

Schueren, L. V., et al. (2012). Polycaprolactone/chitosan blend nanofibres electrospun from an acetic acid/formic acid solvent system. *Carbohydrate Polymers*, *88*, 1221–1226.

Schueren, L. V., Meyer, T. D., et al. (2013). Polycaprolactone and polycaprolactone/chitosan nanofibres functionalised with the pH-sensitive dye Nitrazine Yellow. *Carbohydrate Polymers*, *91*, 284–293.

Shearer, H., & Ellis, M. J. (2006). Effects of common sterilization methods on the structure and properties of poly(D,L-lactic-*co*-glycolic acid) scaffolds. *Tissue Engineering*, *12*, 2717–2727.

Shokrollahi, P., Mehmanchi, M., et al. (2014). Effect of interface on mechanical properties and biodegradation of PCL HAp supramolecular nano-composites. *Journal of Materials Science, Materials in Medicine*, *25*, 23–35.

Teo, W. E., & Ramakrishna, S. (2006). A review on electrospinning design and nanofibre assemblies. *Nanotechnology*, *17*, R81–R106.

Tsai, W. B., Chen, Y-R., et al. (2012). RGD-conjugated UV-crosslinked chitosan scaffolds inoculated with mesenchymal stem cells for bone tissue engineering. *Carbohydrate Polymers*, *89*, 379–387.

Webster, T. J., Massa-Schlueter, E. A., et al. (2004). Osteoblast response to hydroxyapatite doped with divalent and trivalent cations. *Biomaterials*, *25*, 2111–2121.

Woodruff, M. A., & Hutmacher, D. W. (2010). The return of a forgotten polymer: Polycaprolactone in the 21st century. *Progress in Polymer Science*, *35*, 1217–1256.

Wu, H., Wan, Y., et al. (2008). Fabrication of chitosan-*g*-polycaprolactone copolymer scaffolds with gradient porous microstructures. *Materials Letters*, *62*, 2733–2736.

Zhu, Y., Gao, C., Liu, X., & Shen, J. (2002). Surface modification of polycaprolactone membrane via aminolysis and biomacromolecule immobilization for promoting cytocompatibility of human endothelial cells. *Biomacromolecules*, *3*, 1312–1319.